Excitons and two-magnon Raman scattering of the strongly correlated systems La_2CuO_4 and $YBa_2Cu_3O_6$

Eiichi Hanamura,[1] Nguyen Trung Dan,[1,2] and Yukito Tanabe[3]
[1]*Optical Sciences Center, University of Arizona, Tucson, Arizona 85721*
[2]*ERATO Cooperative Excitation Project, Japan Science and Technology Corporation, Tokyo, Japan*
[3]*Department of Applied Physics, University of Tokyo, 7-3-1 Hongo, Bunkyo-ku, Tokyo 113, Japan*
(Received 28 October 1999; revised manuscript received 21 April 2000)

We have solved two problems of strongly correlated electronic systems La_2CuO_4 and $YBa_2Cu_3O_6$: (1) why the lowest-energy absorption peak has stronger oscillator strength than the higher-energy side in La_2CuO_4 while this relative magnitude is reversed in $YBa_2Cu_3O_6$, and (2) why, in both crystals, the two-magnon Raman scattering is observed strongly and resonantly enhanced largely around the high-energy absorption peak or shoulder, while not so appreciable on the low-energy side and around the strongest absorption peak with the lowest excitation energy. In order to treat these problems, an excitonic cluster model in which the bound and unbound states of the charge-transfer exciton are treated on equal footing is proposed to take into account the strong correlation effect of Cu($3d$) electrons and the charge transfer of O($2p$) electrons into the empty Cu($3d$) orbitals.

I. INTRODUCTION

Nonlinear as well as linear optical responses of perovskite-type transition-metal oxides, including La_2CuO_4 and $YBa_2Cu_3O_6$, have been studied extensively, experimentally[1–29] and theoretically.[30–46] Theoretical understanding, however, is still controversial because of the difficulty of describing the competitive behaviors between the strong correlation effect of $3d$ electrons on Cu ions and the itinerant property of the particles and holes involved. This point is in contrast to the case of the corundum-structure transition-metal oxide, e.g., antiferromagnetic (AF) Cr_2O_3, in which the model of localized d electrons works very well as basis states.[47,48] For many perovskite-type transition-metal oxides the effective transfer-matrix elements between the transition-metal $3d$ and the oxygen $2p$ orbitals and the elements between the neighboring oxygen $2p$ orbitals and the binding energy of the charge-transfer (CT) exciton are all of the same order of magnitude. However, the correlation energy of $3d$ electrons and the energy separation between the O($2p$) and Cu($3d$) are much larger. In the present paper, we propose an excitonic cluster model in which the bound and unbound states of the CT excitations from the O $2p$ electron into the empty Cu $3d$ orbital are equally taken into account using the characteristics mentioned above.

So far, the small exciton model has been adopted in order to explain the large dispersions of CT excitations observed by angle-resolved electron-energy-loss spectroscopy in $Sr_2CuO_2Cl_2$, where the same CuO_2 plane responds to the visible light.[26] Zhang and Ng[45] concluded that the dipole-allowed CT exciton has a dispersion as large as 1.5 eV because the bound exciton of a spin singlet can move through the lattice freely without disturbing the AF spin background. For this reason, they obtained exciton dispersion by neglecting the AF *A*- and *B*- sublattice structure of the system. In their research, the free electron and hole propagation was completely neglected. On the other hand, Chubukov and Frenkel[43] proposed, in order to explain the mystery of two-magnon Raman scattering (RS), the band-to-band transition model of the Mott-Hubbard system. In this model, the Raman tensor is expanded to the second order in the intraband fermion-magnon interactions, and multiple resonance is found to be responsible for the enhancement on the high-energy side. However, the CT between Cu and O ions and the exciton effects were completely neglected.

In the present paper, we treat both the bound and unbound states of the CT exciton on the same footing. Therefore, we take into account also the contribution of the band-to-band transitions to these optical responses. For this purpose, the model of an excitonic cluster is proposed in Sec. II. By adopting this model, we will be able to understand the two following problems. First, the exciton effect is stronger than the itinerant nature in La_2CuO_4, while the opposite is true for $YBa_2Cu_3O_6$. This is seen in the absorption peak of the lowest-energy exciton which is stronger than the band-to-band transitions on the high-energy side in La_2CuO_4, while the oscillator strength distributes oppositely in $YBa_2Cu_3O_6$. This effect is discussed in the first and second part of Sec. III. Second, we can solve the mystery of why the two-magnon RS is so strongly observable. Further, we can find the reason why the two-magnon RS is not resonantly enhanced even when the frequency of the incident light approaches the strongest absorption peak with the lowest excitation energy, but is resonantly enhanced when it becomes close to the weaker absorption peak or shoulder on the higher-energy side in both crystals. This will be discussed in the third part of Sec. III. Section IV is devoted to the discussion and the listing of several future problems.

II. HAMILTONIAN AND BASIS STATES

A. Mott-Hubbard Hamiltonian

We confine ourselves in the present paper to cuprates La_2CuO_4 and $YBa_2Cu_3O_6$ which are parent crystals of high-

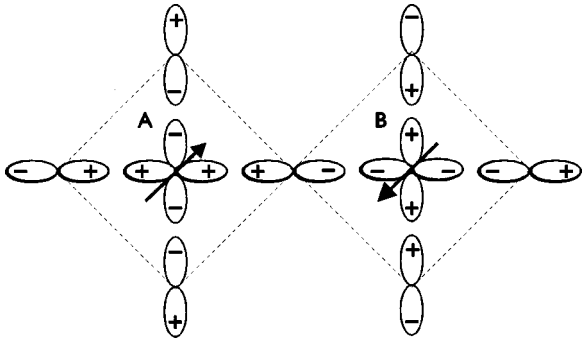

FIG. 1. Schematic diagram of the hybridization of the O $2p_{x,y}$ and Cu $3d_{x^2-y^2}$ orbitals. The signs + and − represent the phase of wave functions of O $2p_{x,y}$ orbitals around Cu $3d_{x^2-y^2}$ orbitals in *A* and *B* sublattices.

temperature superconductors. These are AF insulators at and below room temperature. The low-lying optical excitation of these crystals in the visible region is known to be determined by the CuO_2 plane. The relevant orbitals, i.e., Cu $(3d_{x^2-y^2})$ of *A* and *B* sublattices in the AF structure and O $(2p_\sigma = 2p_{x,y})$ surrounding these are drawn in Fig. 1 together with the phases of these wave functions chosen in this paper.

We have found that the three-band Mott-Hubbard Hamiltonian can describe optical responses of La_2CuO_4 and its family in the visible region.[49] The three bands consist of O $2p_{x,y}$ or $2p_\sigma$ with its energy E_p+U_p, singly and doubly occupying Cu $3d_{x^2-y^2}$ levels with energies E_d and E_d+U, respectively. We start from the following modified three-band Hubbard Hamiltonian in the electron picture:

$$H_{el}=\sum_{i,\sigma} E_d a^\dagger_{i\sigma}a_{i\sigma}+\sum_{l,\sigma} E_p b^\dagger_{l\sigma}b_{l\sigma}+H'_{el}+U\sum_i a^\dagger_{i\uparrow}a_{i\uparrow}a^\dagger_{i\downarrow}a_{i\downarrow}$$
$$+U_p\sum_l b^\dagger_{l\uparrow}b_{l\uparrow}b^\dagger_{l\downarrow}b_{l\downarrow}+V\sum_{i\sigma\sigma'}\sum_{l\in\{i\}} a^\dagger_{i\sigma}a_{i\sigma}b^\dagger_{l\sigma'}b_{l\sigma'}, \tag{2.1}$$

$$H'_{el}=\sum_{i\sigma}\sum_{l\in\{i\}} V_{il}a^\dagger_{i\sigma}b_{l\sigma}+\sum_{l\sigma}\sum_{l'\in\{l\}} V_{ll'}b^\dagger_{l\sigma}b_{l'\sigma}. \tag{2.2}$$

Here U and U_p are the on-site Coulomb repulsion at a Cu and an O site, respectively, and V is the Cu-O interatomic Coulomb repulsion between the nearest-neighbor Cu and O ions. The hybridization matrix V_{il} between the nearest neighbor O $2p_\sigma$ and Cu $3d_{x^2-y^2}$ orbitals $(l\in\{i\})$ and the charge transfer $V_{ll'}$ of the O $(2p)$ electron between the neighboring O $2p_\sigma$ orbitals $(l'\in\{l\})$ are described by t_0 and t_p, respectively. Strictly speaking, the Hamiltonian (2.1) describes a four-band model because O $2p_\sigma$ has the energy E_p+U_p or E_p depending on the configuration $O(2p)^6$ or $O(2p)^5$, but the contribution from $O(2p)^5$ is almost negligible in the evaluation of the E_u symmetry state, so that we may regard our system effectively as the three-band model. The electronic ground state described by the Hamiltonian (2.1) and (2.2) of both undoped La_2CuO_4 and $YBa_2Cu_3O_6$ has one $(3d_{x^2-y^2})$ electron per Cu^{2+} ion and two $2p_\sigma$ electrons per O^{2-} ion. Note that this electron picture is equivalent to the conventional hole picture for Cu$(3d)$ and O$(2p)$ with hole

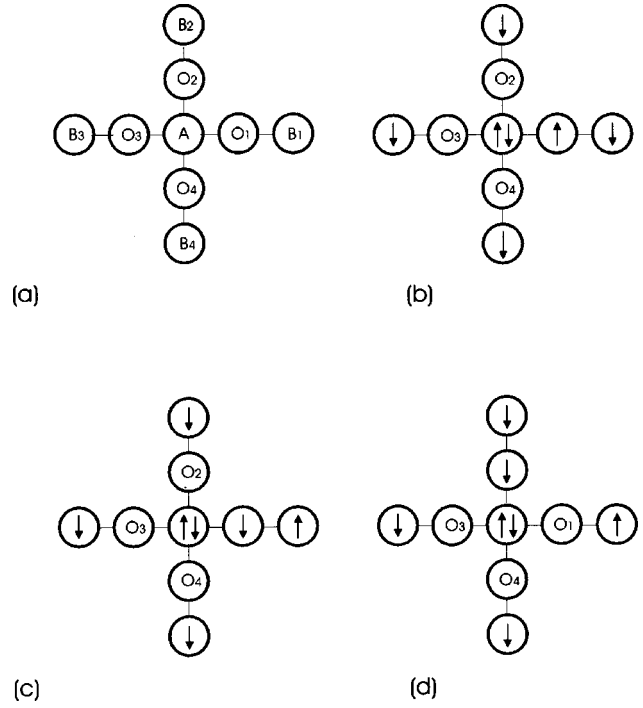

FIG. 2. (a) Notations and numbering of *A*- and *B*- sublattice copper ions and oxygen ions, (b) one of the charge-transfer excitations $\psi^A(1,0)$ in which a down-spin electron in the $2p_x$ orbital of the O_1 $[O^{2-}(1,0)]$ ion is transferred to the *A*-sublattice Cu ion, (c) $\psi^A_{(2,0)}(1,0)$ in which two electrons, i.e., an up-spin electron in $O_1[O^-(1,0)]$ $2p_x$ and a down-spin $3d_{x^2-y^2}$ electron on the nearest-neighbor $B_1[Cu(2,0)]$ ion of the *B* sublattice are exchanged, and (d) $\psi^A_{(2,0)}(0,1)$ in which an up-spin electron in $O_2[O^-(0,1)]2p_y$ has propagated into a $2p_x$ orbital at O_1 in (c).

energies ε_d and ε_p, respectively, if we set $E_d+U=-\varepsilon_d$ and $E_p+U_p+2V=-\varepsilon_p$. We have chosen the electron picture because it makes the physical understanding much easier.

B. Excitonic cluster model

We will consider the case of La_2CuO_4 and $YBa_2Cu_3O_6$ which satisfy $t_p<t_0\ll U+E_d-E_p-U_p$ and $E_p+U_p-E_d$. Therefore, we are justified to expand the physical quantities in terms of $t_0/(U-E_p-U_p)$ and $t_0/(E_p+U_p)$ by choosing the origin of energy at $E_d=0$. Under this condition, the electronic ground state around the AF *A* sublattice may be described as in Fig. 2(a). This figure depicts the $Cu^{2+}(3d)^9$, with its up-spin $3d_{x^2-y^2}$ electron surrounded by four $O^{2-}(2p)^6$ ions as the nearest neighbor and four $Cu^{2+}(3d)^9$ ions of *B* sublattice as the second-nearest neighbors. The radiation field can induce the CT excitations as seen in the example in Fig. 2(b) through the transition dipole moment operator

$$\boldsymbol{P}=\sum_{i\sigma}\sum_{l\in\{i\}}\boldsymbol{\mu}_{il}b^\dagger_{l,\sigma}a_{i,\sigma}+\text{h.c.}, \tag{2.3}$$

where the transition dipole moment $\boldsymbol{\mu}_{il}$ is linearly proportional to t_0 and also to the unit vector drawn from the ith lattice point to the lth. In Fig. 2(b) the down-spin electron on O_1 is transferred to the copper ion *A* at the center by the x component P_x. The corresponding excited state will be de-

TABLE I. Examples of basis functions in site representation. The vacuum state $|0\rangle$ is defined by the product of O $(2p)^4$ and Cu $(3d)^8$ in which two $2p_\sigma$ electrons and $3d_{x^2-y^2}\uparrow$ and $3d_{x^2-y^2}\downarrow$ electrons are missing. For simplicity, we have introduced the notation $|0\rangle'$. It represents the state where the ions of the system are left in the same state as in $|g\rangle$, except for those at (0,0), (1,0), and (2,0), whose $3d_{x^2-y^2}$ and $2p_\sigma$ orbitals are empty as in the vacuum state.

$$|g\rangle=\prod_{m+n=\text{even}}^{A} d_\uparrow^\dagger(2m,2n)\prod_{m+n=\text{odd}}^{B} d_\downarrow^\dagger(2m,2n)\prod_{m+n=\text{odd}} p_\uparrow^\dagger(m,n)\ p_\downarrow^\dagger(m,n)\ |0\rangle$$

$$\psi^A(1,0)=d_{A\downarrow}^\dagger(0,0)p_\downarrow(1,0)\ |g\rangle$$

$$=d_{A\uparrow}^\dagger(0,0)d_{A\downarrow}^\dagger(0,0)d_{B\downarrow}^\dagger(2,0)p_\uparrow^\dagger(1,0)\ |0\rangle'$$

$$\psi^A_{(2,0)}(1,0)=d_{A\downarrow}^\dagger(0,0)p_\uparrow(1,0)d_{B\uparrow}^\dagger(2,0)d_{B\downarrow}(2,0)\ |g\rangle$$

$$=-d_{A\uparrow}^\dagger(0,0)d_{A\downarrow}^\dagger(0,0)d_{B\uparrow}^\dagger(2,0)p_\downarrow^\dagger(1,0)\ |0\rangle'$$

$$=-p_\downarrow^\dagger(1,0)p_\uparrow(1,0)d_{B\uparrow}^\dagger(2,0)d_{B\downarrow}(2,0)\ \psi^A(1,0)$$

$$\psi^A_{(2,0)}(0,1)=d_{A\downarrow}^\dagger(0,0)p_\uparrow(0,1)d_{B\uparrow}^\dagger(2,0)d_{B\downarrow}(2,0)\ |g\rangle$$

noted as $\psi^A(1,0)$. Reflecting D_{4h} symmetry of the CuO_2 plane, we have four equivalent CT excitations: $\psi^A(1,0),\psi^A(0,1),\psi^A(-1,0)$, and $\psi^A(0,-1)$ around the *A*-sublattice Cu ions and $\psi^B(1,0),\psi^B(0,1),\psi^B(-1,0)$, and $\psi^B(0,-1)$ around the *B*-sublattice Cu ions, both of which are connected by the electronic dipole transition from the electronic and magnetic ground state. Here and hereafter we assume the AF, i.e., the Néel state, for the magnetic ground state. When two electrons of $O_1(2p_x\uparrow)$ and B_1 Cu$(3d_{x^2-y^2}\downarrow)$ are exchanged through the perturbation process of the second order in t_0, i.e., the Zhang-Rice mechanism,[32] we have an excited state called the exchanged state. This is shown in Fig. 2(c) and is represented as $\psi^A_{(2,0)}(1,0)$, where the two-dimensional argument (1,0) denotes the hole coordinate as above and the suffix (2,0) gives the position of the reversed spin (on the *B* sublattice) of the CuO_2 plane. We have four equivalent excitations $\psi^{A,B}_{(2,0)}(1,0),\psi^{A,B}_{(0,2)}(0,1),\psi^{A,B}_{(-2,0)}(-1,0)$, and $\psi^{A,B}_{(0,-2)}(0,-1)$ around both the *A*- and *B*-sublattice Cu ions. When these are radiatively annihilated by the electric dipole interaction, the result will be the reversal of the orientation of a spin pair on the $A(B)$ sublattice (0,0) and the $B(A)$ sublattice (2,0), $(-2,0),(0,2)$, or $(0,-2)$. These states correspond to two-magnon excitation in the electronic ground state. These two kinds of CT states can contribute strongly to the linear optical-absorption and two-magnon RS processes in the site representation. However, the hole, i.e., $O^-(2p)^5$ configuration in the CT excitation, can propagate into any other (i,j) site relative to the electron, i.e., the $Cu^+(3d)^{10}$ configuration at the origin (0,0), by the repeated application of the process of the second order in t_0 and/or the first order in t_p [e.g., see Fig. 2(d)]. Fortunately, only the configuration in which the electron $[Cu^+(3d)^{10}]$ and the hole $[O^-(2p)^5]$ are in the nearest neighbors will contribute to the optical response, so that these higher-order configurations in t_0 and t_p may be treated as perturbations as seen in this paper. The wave functions given in Fig. 2 are expressed in Table I in the second quantized form for reference to make our phase choice clearer.

There are too many basis states in this site representation when we take into account the higher-order processes of t_0^2 and t_p. Therefore, to simplify the diagonalizing of the energy matrix, one should make the best use of the symmetry of D_{4h} in our system. At first, four dipole-allowed states around the $A(B)$ sublattice are mixed with each other by the second-order process in t_0, i.e., $t_1=t_0^2/(U-V-U_p-E_p)$ and t_p. When we diagonalize the eigen equation

$$\begin{pmatrix} E_0 & t_1+t_p & t_1 & t_1+t_p \\ t_1+t_p & E_0 & t_1+t_p & t_1 \\ t_1 & t_1+t_p & E_0 & t_1+t_p \\ t_1+t_p & t_1 & t_1+t_p & E_0 \end{pmatrix}\begin{pmatrix} \psi^A(1,0) \\ \psi^A(0,1) \\ \psi^A(-1,0) \\ \psi^A(0,-1) \end{pmatrix}$$

$$=E\begin{pmatrix} \psi^A(1,0) \\ \psi^A(0,1) \\ \psi^A(-1,0) \\ \psi^A(0,-1) \end{pmatrix}, \tag{2.4}$$

we obtain the eigenfunctions and eigenenergies of the four CT states

$$\Psi^1_{aA}=\frac{1}{2}\{\psi^A(1,0)+\psi^A(0,1)+\psi^A(-1,0)+\psi^A(0,-1)\},$$

$$E_0+3t_1+2t_p,$$

$$\Psi^1_{bA}=\frac{1}{2}\{\psi^A(1,0)-\psi^A(0,1)+\psi^A(-1,0)-\psi^A(0,-1)\},$$

$$E_0-t_1-2t_p,$$

$$\Psi^1_{exA}=\frac{1}{\sqrt{2}}\{\psi^A(1,0)-\psi^A(-1,0)\},\qquad E_0-t_1,$$

$$\Psi^1_{eyA}=\frac{1}{\sqrt{2}}\{\psi^A(0,1)-\psi^A(0,-1)\},\qquad E_0-t_1. \tag{2.5}$$

Here the diagonal energy E_0 is evaluated to the fourth order in t_0, i.e., to the order of J the superexchange energy which induces the AF structure, in addition to the exchange energy to the second order in t_0,

$$E_0 \equiv U - E_p - U_p - V + t_1 - t_1' - t_2' + J, \tag{2.6}$$

where

$$t_1' = \frac{t_0^2}{U - E_p - U_p - 2V}, \tag{2.7}$$

$$t_2 = \frac{t_0^2}{E_p + U_p}, \quad t_2' = \frac{t_0^2}{E_p + U_p + V}, \tag{2.8}$$

and

$$J = \frac{4t_0^4}{(U - E_p - U_p - V)^2}\left[\frac{1}{U} + \frac{1}{2(U - E_p - U_p - 2V)}\right]. \tag{2.9}$$

Thus we have four states $A_{1g}(\Psi_{aA}^1)$, $B_{1g}(\Psi_{bA}^1)$, and twofold degenerate $E_u(\Psi_{exA}^1$ and $\Psi_{eyA}^1)$ around the A sublattice, that are symmetry adapted according to the irreducible representations of the group D_{4h}. We have also similar expressions for the eigenfunctions and eigenenergies around the B sublattice. Among these, only the states with E_u symmetry will contribute to the linear absorption and two-magnon RS. Furthermore, the states with the same symmetry in the site representation are mixed with each other through the charge-transfer processes involving t_0 and t_p. Therefore, only the basis functions with E_u symmetry which are made by the higher-order processes in t_0 and t_p will be considered hereafter. The basis functions corresponding to Fig. 2(c) are derived as

$$\Psi_{exA}^1(0) = \frac{1}{\sqrt{2}}\{\psi_{(2,0)}^A(1,0) - \psi_{(-2,0)}^A(-1,0)\}, \tag{2.10}$$

$$\Psi_{eyA}^1(0) = \frac{1}{\sqrt{2}}\{\psi_{(0,2)}^A(0,1) - \psi_{(0,-2)}^A(0,-1)\}, \tag{2.11}$$

where the two-dimensional argument of the wave functions on the right-hand side, e.g., (1,0) describes the hole position of $O(2p)$[5] relative to that of the electron $Cu(3d)$[10]. The two-dimensional (2D) suffix gives the position of the reversed spin which is induced by the exchange of the $O(2p_\sigma\uparrow)$ electron with the nearest $Cu(3d_{x^2-y^2}\downarrow)$ electron in the same manner as previously explained. The argument (0) of the function on the left-hand side was introduced to indicate that the hole is located at the neighboring oxygen ion that is closest to the *reversed spin*. When the hole is located at the second closest oxygen ion, argument (1) will be used and so on [see below, Eqs. (2.16)–(2.21)]. No argument means no reversed spin.

When the oxygen hole propagates to the second and third-nearest neighbors of the (0,0) site, it will give rise to the following states with E_u symmetry:

$$\Psi_{exA}^2 = \frac{1}{2}\{\psi^A(2,1) + \psi^A(2,-1) - \psi^A(-2,1) - \psi^A(-2,-1)\}, \tag{2.12}$$

$$\Psi_{eyA}^2 = \frac{1}{2}\{\psi^A(1,2) + \psi^A(-1,2) - \psi^A(1,-2) - \psi^A(-1,-2)\}, \tag{2.13}$$

$$\Psi_{exA}^3 = \frac{1}{\sqrt{2}}\{\psi^A(3,0) - \psi^A(-3,0)\}, \tag{2.14}$$

$$\Psi_{eyA}^3 = \frac{1}{\sqrt{2}}\{\psi^A(0,3) - \psi^A(0,-3)\}. \tag{2.15}$$

These states in Eqs. (2.12)–(2.15) are obtained from Ψ_{exA}^1 and Ψ_{eyA}^1 after applying two steps of CT involving t_0, i.e., they are states, perturbationally, by t_0^2 higher than Ψ_{exA}^1 and Ψ_{eyA}^1. To the next higher order in t_0, i.e., in t_0^4, we must include the following states with the electron and the hole still in the nearest neighbor but with the hole $[O(2p_\sigma\downarrow)]$ and the reversed spin (the magnon) propagating away from the original locations given in the states $\Psi_{exA}^1(0)$ or $\Psi_{eyA}^1(0)$ [See Fig. 2(d)]:

$$\Psi_{exA}^1(2) = \frac{1}{\sqrt{2}}\{\psi_{(2,0)}^A(-1,0) - \psi_{(-2,0)}^A(1,0)\}, \tag{2.16}$$

$$\Psi_{eyA}^1(2) = \frac{1}{\sqrt{2}}\{\psi_{(0,2)}^A(0,-1) - \psi_{(0,-2)}^A(0,1)\}, \tag{2.17}$$

$$\Psi_{exA}^1(1) = \frac{1}{2}\{\psi_{(2,0)}^A(0,1) - \psi_{(-2,0)}^A(0,1) + \psi_{(2,0)}^A(0,-1) - \psi_{(-2,0)}^A(0,-1)\}, \tag{2.18}$$

$$\Psi_{eyA}^1(1) = \frac{1}{2}\{\psi_{(0,2)}^A(1,0) - \psi_{(0,-2)}^A(1,0) + \psi_{(0,2)}^A(-1,0) - \psi_{(0,-2)}^A(-1,0)\}, \tag{2.19}$$

$$\Psi_{e'xA}^1(1) = \frac{1}{2}\{\psi_{(0,2)}^A(1,0) + \psi_{(0,-2)}^A(1,0) - \psi_{(0,2)}^A(-1,0) - \psi_{(0,-2)}^A(-1,0)\}, \tag{2.20}$$

$$\Psi_{e'yA}^1(1) = \frac{1}{2}\{\psi_{(2,0)}^A(0,1) + \psi_{(-2,0)}^A(0,1) - \psi_{(2,0)}^A(0,-1) - \psi_{(-2,0)}^A(0,-1)\}. \tag{2.21}$$

Note that the magnon (the reversed spin) has propagated by two steps in t_0 in forming $\Psi_{exA}^1(2)$, starting from $\Psi_{exA}^1(0)$, while $\Psi_{exA}^1(1)$ can be reached by one step in t_p or two steps in t_0 also starting from $\Psi_{exA}^1(0)$. Although the last two states $\Psi_{e'x,yA}^1(1)$ given by Eqs. (2.20) and (2.21) are also obtained

by one step in t_p or two steps in t_0 from $\Psi^1_{ex,yA}(0)$, they are found to have no mixing through H' with other states and no contribution to the linear absorption and two-magnon RS. Therefore we will discard these states, $\Psi^1_{e'xA}(1)$ and $\Psi^1_{e'yA}(1)$, from our consideration in the present treatment of optical responses.

When we exchange the hole $O(2p)^5$ ($2p_x\uparrow$ electron) in Ψ^2_{exA} and Ψ^3_{exA} and the nearest-neighbor $Cu(3d)^9$ in the B sublattice ($3d_{x^2-y^2}\downarrow$ electron), we have the following states which are by t_0^4 higher than Ψ^1_{exA} and Ψ^1_{eyA}, i.e., of the same order in t_0 as the states of Eqs. (2.16)–(2.21),

$$\Psi^2_{exA}(0)=\frac{1}{2}\{\psi^A_{(2,0)}(2,1)+\psi^A_{(2,0)}(2,-1)-\psi^A_{(-2,0)}(-2,1)-\psi^A_{(-2,0)}(-2,-1)\}, \tag{2.22}$$

$$\Psi^2_{eyA}(0)=\frac{1}{2}\{\psi^A_{(0,2)}(1,2)+\psi^A_{(0,2)}(-1,2)-\psi^A_{(0,-2)}(1,-2)-\psi^A_{(0,-2)}(-1,-2)\}, \tag{2.23}$$

$$\Psi^3_{exA}(0)=\frac{1}{\sqrt{2}}\{\psi^A_{(2,0)}(3,0)-\psi^A_{(-2,0)}(-3,0)\}, \tag{2.24}$$

$$\Psi^3_{eyA}(0)=\frac{1}{\sqrt{2}}\{\psi^A_{(0,2)}(0,3)-\psi^A_{(0,-2)}(0,-3)\}. \tag{2.25}$$

To this order, we must also include the following three sets of states:

$$\Psi^4_{exA}=\frac{1}{2}\{\psi^A(3,2)+\psi^A(3,-2)-\psi^A(-3,2)-\psi^A(-3,-2)\}, \tag{2.26}$$

$$\Psi^4_{eyA}=\frac{1}{2}\{\psi^A(2,3)+\psi^A(2,-3)-\psi^A(-2,3)-\psi^A(-2,-3)\}, \tag{2.27}$$

$$\Psi^5_{exA}=\frac{1}{2}\{\psi^A(4,1)+\psi^A(4,-1)-\psi^A(-4,1)-\psi^A(-4,-1)\}, \tag{2.28}$$

$$\Psi^5_{eyA}=\frac{1}{2}\{\psi^A(1,4)+\psi^A(-1,4)-\psi^A(1,-4)-\psi^A(-1,-4)\}, \tag{2.29}$$

$$\Psi^6_{exA}=\frac{1}{\sqrt{2}}\{\psi^A(5,0)-\psi^A(-5,0)\}, \tag{2.30}$$

$$\Psi^6_{eyA}=\frac{1}{\sqrt{2}}\{\psi^A(0,5)-\psi^A(0,-5)\}. \tag{2.31}$$

The basis functions $\Psi^n_{exA}(0)$ $(n=4,5,6)$ in which two electrons are exchanged between $[O(2p)^5,2p_\sigma\uparrow]$ and the nearest-neighbor B sublattice $[Cu(3d)^9,3d_{x^2-y^2}\downarrow]$ are obtained from the above equations, though these states are by t_0^6 order higher than Ψ^1_{exA}. We must also repeat these procedures around the B sublattice. Since only the symmetric state with respect to the interchange of A and B sublattices can contribute to the optical responses, we finally obtain the eigenstates belonging to the eigenenergy E_i of the CT excitation as a symmetric linear combination of the states with the same symmetry species,

$$\begin{aligned}\Psi_{ex+}[i]=&a_i[ex]\Psi^1_{ex+}+b_i[ex]\Psi^1_{ex+}(0)+c_i[ex]\Psi^1_{ex+}(2)\\&+d_i[ex]\Psi^1_{ex+}(1)+e_i[ex]\Psi^2_{ex+}\\&+f_i[ex]\Psi^2_{ex+}(0)+g_i[ex]\Psi^3_{ex+}\\&+h_i[ex]\Psi^3_{ex+}(0)+j_i[ex]\Psi^4_{ex+}\\&+k_i[ex]\Psi^4_{ex+}(0)+l_i[ex]\Psi^5_{ex+}\\&+m_i[ex]\Psi^5_{ex+}(0)+\cdots,\end{aligned} \tag{2.32}$$

where

$$\Psi^n_{ex+}=\frac{1}{\sqrt{2}}\{\Psi^n_{exA}+\Psi^n_{exB}\},$$

$$\Psi^n_{ex+}(i)=\frac{1}{\sqrt{2}}\{\Psi^n_{exA}(i)+\Psi^n_{exB}(i)\}. \tag{2.33}$$

C. Energy matrix and its diagonalization

Let us first give the secular equation to obtain the eigenenergies $\{E_i\}$ and the corresponding eigenfunctions $\{\Psi_{ex+}[i]\}$ in terms of the set of basis functions:

$$\{\Psi^1_{ex+},\Psi^1_{ex+}(0),\Psi^1_{ex+}(2),\Psi^1_{ex+}(1),\Psi^2_{ex+},\Psi^2_{ex+}(0),\Psi^3_{ex+},\Psi^3_{ex+}(0),\Psi^4_{ex+},\Psi^4_{ex+}(0),\Psi^5_{ex+},\Psi^5_{ex+}(0),\ldots\}. \tag{2.34}$$

Here the charge-transfer effect H' in Eq. (2.2) is taken into account by the degenerate perturbation method, and the off-diagonal matrix element is evaluated to the first order in t_p and to the second order in t_0. The diagonal component is evaluated to the fourth order in t_0 as mentioned in the preceding subsection. Note that these bases are the states with a single excitation, i.e., one electron $Cu(3d_{x^2-y^2})^{10}$ and one

TABLE II. Material constants for (a) La_2CuO_4 and (b) $YBa_2Cu_3O_6$.

	U	U_p	E_p	t_0	t_p	V	J
La_2CuO_4	10.0	3.5	3	0.82	0.40	0.50	0.14
$YBA_2Cu_3O_6$	10.0	3.4	3	1.0	0.55	0.35	0.12

hole $O(2p)^5$, while the intermediate states in evaluating the perturbational effects of H' are those with two or zero excitations.

The secular equation we have used in the present paper now reads

$$M\Phi = E\Phi, \tag{2.35}$$

where

$$M=\begin{pmatrix} H_{I,I} & H_{I,II} & H_{I,III} \\ H_{II,I} & H_{II,II} & H_{II,III} \\ H_{III,I} & H_{III,II} & H_{III,III} \end{pmatrix}, \qquad \Phi=\begin{pmatrix} a_i[ex] \\ b_i[ex] \\ c_i[ex] \\ \cdots \\ m_i[ex] \end{pmatrix}, \tag{2.36}$$

with

$$H_{I,I}=\begin{pmatrix} \varepsilon_0-t_1'-t_2 & -t_2' & 0 & 0 \\ -t_2' & \varepsilon_0'-t_2' & t_1' & \sqrt{2}(t_p-t_1') \\ 0 & t_1' & \varepsilon_0'+t_1 & \sqrt{2}(t_p-t_1) \\ 0 & \sqrt{2}(t_p-t_1') & \sqrt{2}(t_p-t_1) & \varepsilon_0'+2t_1 \end{pmatrix}, \tag{2.37}$$

$$H_{I,II}=\begin{pmatrix} \sqrt{2}(t_p-\tau) & -\sqrt{2}(\gamma+\tau) & -\tau & -(2\gamma+\tau) \\ -\sqrt{2}(\gamma+\tau) & \sqrt{2}(t_p-\tau) & -(\gamma+\tau) & -\tau \\ 0 & 0 & \gamma & 0 \\ \gamma & 0 & 0 & 0 \end{pmatrix}, \tag{2.38}$$

$$H_{I,III}=\begin{pmatrix} 0 & 0 & 0 & 0 \\ 0 & 0 & 0 & 0 \\ 0 & 0 & 0 & 0 \\ 0 & 0 & 0 & 0 \end{pmatrix}, \tag{2.39}$$

$$H_{II,II}=\begin{pmatrix} \varepsilon_1-t_3-2t_2 & -(t_1'+2t_2+t_3) & \sqrt{2}(t_p-t_2) & -\sqrt{2}(t_1'+t_2) \\ -(t_1'+2t_2+t_3) & \varepsilon_1'-2t_3-3t_2 & -\sqrt{2}(t_1'+t_2) & \sqrt{2}(t_p-t_2) \\ \sqrt{2}(t_p-t_2) & -\sqrt{2}(t_1'+t_2) & \varepsilon_1-t_2-t_3 & -t_2-t_3 \\ -\sqrt{2}(t_1'+t_2) & \sqrt{2}(t_p-t_2) & -t_2-t_3 & \varepsilon_1'-2(t_2+t_3) \end{pmatrix}, \tag{2.40}$$

$$H_{II,III}=\begin{pmatrix} t_p-t_1' & 0 & 0 & 0 \\ 0 & 0 & 0 & 0 \\ 0 & 0 & \sqrt{2}(t_p-t_1') & 0 \\ 0 & 0 & 0 & 0 \end{pmatrix}, \tag{2.41}$$

$$H_{III,III}=\begin{pmatrix} \varepsilon_1-t_2-t_3 & -t_2-t_3 & t_p-t_2 & -t_1'-t_2 \\ -t_2-t_3 & \varepsilon_1'-2(t_2+t_3) & -t_1'-t_2 & t_p-t_2 \\ t_p-t_2 & -t_1'-t_2 & \varepsilon_1-t_1'-t_2-t_3 & -t_2-t_3 \\ -t_1'-t_2 & t_p-t_2 & -t_2-t_3 & \varepsilon_1'-2(t_3+t_2) \end{pmatrix}. \tag{2.42}$$

In these equations, we have set

$$\varepsilon_0=U-U_p-E_p-V+J \quad \text{and} \quad \varepsilon_0'=\varepsilon_0+\frac{3}{2}J, \tag{2.43}$$

$$\varepsilon_1=\varepsilon_0+V \quad \text{and} \quad \varepsilon_1'=\varepsilon_1+\frac{3}{2}J, \tag{2.44}$$

$$\gamma=\frac{1}{2}(t_1'+t_1''), \quad \tau=\frac{1}{2}(t_2+t_2'), \tag{2.45}$$

and

$$t_1''=\frac{t_0^2}{U-E_p-U_p-3V}, \quad t_3=\frac{t_0^2}{U-E_p-2V}. \tag{2.46}$$

TABLE III. The eigenenergies and eigenfunctions for La_2CuO_4.

E_i (eV)	a_i	b_i	c_i	d_i	e_i	f_i	g_i	h_i	j_i	k_i	l_i	m_i
1.96	0.12	-0.62	-0.21	0.53	-0.46	0.14	-0.04	0.20	0.06	0.00	0.02	0.01
2.12	0.77	0.13	-0.08	-0.03	-0.02	0.33	0.34	0.38	0.02	-0.02	-0.09	-0.01
2.80	0.20	-0.27	0.21	-0.06	0.44	0.68	-0.17	-0.20	-0.23	0.12	0.29	-0.08
2.86	0.30	-0.14	0.18	0.01	-0.14	-0.38	-0.40	0.32	-0.14	0.29	0.57	-0.02
3.02	0.19	-0.19	0.65	-0.36	-0.27	0.04	-0.18	-0.18	0.29	-0.19	-0.24	0.23
3.19	0.01	-0.24	-0.08	0.24	0.42	-0.07	-0.37	0.41	0.00	-0.50	-0.22	0.31
3.24	0.04	-0.15	0.18	-0.02	-0.03	-0.12	-0.11	0.10	-0.41	-0.07	-0.44	-0.74
3.43	0.05	0.11	-0.09	-0.09	-0.24	-0.03	0.15	-0.20	-0.62	-0.60	0.29	0.18
4.05	0.39	0.33	-0.36	0.02	0.01	0.00	-0.58	-0.49	0.10	-0.07	-0.08	-0.11
4.66	0.08	0.00	0.00	0.02	0.02	-0.06	-0.05	-0.09	-0.53	0.50	-0.44	0.51
5.50	0.14	0.31	0.52	0.68	0.23	-0.15	0.17	-0.22	0.04	0.02	0.03	0.02
5.91	0.29	-0.41	-0.12	0.24	0.46	-0.47	0.34	-0.35	0.05	-0.02	0.05	-0.02

We diagonalize the charge-transfer matrix M, Eq. (2.36) with the basis states corresponding up to the nth nearest-neighbor electron-hole pair. When the change in the eigenfunctions and eigenenergies below 3 eV is negligible between the nth- and the $(n-1)$th-neighbor basis functions, we concluded the convergence as sufficient at such a value of n. Then we used the obtained results to calculate the absorption spectra and resonance enhancement spectra of two-magnon RS of La_2CuO_4 and $YBa_2Cu_3O_6$ as shown in the next section. Material constants used here are listed in Table II and their values are close to those obtained by other groups.[31,34–36,38,50–53] Eigenenergies and eigenvectors $\{a_i, b_i, \ldots, m_i\}$ are listed for La_2CuO_4 and $YBa_2Cu_3O_6$ in Tables III and IV, respectively.

III. OPTICAL ABSORPTION AND TWO-MAGNON RS

A. Optical responses of the two systems

Before going into the details of the calculation of linear absorption and two-magnon RS resonance-enhancement spectra, let us consider the difference between the optical responses of the bound and unbound states expected for the two systems, i.e., La_2CuO_4 and $YBa_2Cu_3O_6$. This difference is closely related to the observed features of both of the spectra shown in Figs. 3 and 4.

When the excitonic effect V is much stronger than t_p and the second-order effect of t_0, the excitation is well localized within a unit cell so that the optical response can be described by $\{\Psi^1_{ex+}, \Psi^1_{ex+}(0), \Psi^1_{ex+}(2), \Psi^1_{ex+}(1)\}$ as bases. This is almost the case of La_2CuO_4, and both the spectra of linear absorption and the two-magnon RS resonance enhancement could be described in terms of these four basis functions.[49] For La_2CuO_4, the large absorption peak observed on the lowest-energy side corresponds to the dipole-allowed state Ψ^1_{ex+} and the weak shoulder on the high-energy side comes mainly from the hybridization of the dipole-allowed state onto the $\Psi^1(0)$ state through the second-order exchange effect in t_0. However, when we take into account the mixing of the unbound electron-hole states Ψ^2_{ex+} and Ψ^3_{ex+} onto Ψ^1_{ex+} through t_p and t_0^2 terms, a better agreement between the theory and the observation is obtained. This is because part of the oscillator strength, though small, moves from the lowest bound CT exciton into the unbound states on the high-energy side.

When the CT effect t_p and t_1, t_1', t_2, or t_2' become the same order of magnitude or larger than the excitonic binding energy V, a large part of the oscillator strength is removed onto the unbound states Ψ^n_{ex+} and $\Psi^n_{ex+}(0)$ $(n \geqslant 2)$. This is the case of $YBa_2Cu_3O_6$. However, the contributions from the states with larger electron-hole separation n are reduced as n

TABLE IV. The eigenenergies and eigenfunctions for $YBa_2Cu_3O_6$.

E_i(eV)	a_i	b_i	c_i	d_i	e_i	f_i	g_i	h_i	j_i	k_i	l_i	m_i
1.62	0.30	0.53	0.09	-0.38	0.47	0.17	0.18	0.43	-0.05	-0.02	-0.03	-0.02
1.73	0.60	-0.27	-0.19	0.28	-0.25	0.47	0.36	0.14	0.05	-0.03	-0.11	0.00
2.30	0.24	0.19	-0.07	0.01	-0.45	-0.70	0.06	0.39	0.15	-0.04	-0.12	0.07
2.51	0.25	-0.15	0.05	0.07	0.02	-0.06	-0.27	0.23	-0.16	0.47	0.73	-0.03
2.76	0.33	-0.01	0.21	-0.16	-0.04	0.12	-0.07	-0.10	0.51	-0.07	0.18	0.77
2.85	0.19	-0.35	0.06	0.20	0.30	-0.06	-0.47	0.37	-0.20	-0.54	-0.13	0.15
2.92	0.23	-0.16	0.66	-0.40	-0.29	0.05	-0.22	-0.17	-0.06	-0.01	-0.18	-0.28
3.09	0.20	0.19	-0.11	-0.12	-0.26	-0.01	0.23	-0.23	-0.57	-0.49	0.40	0.20
3.90	0.43	0.37	-0.41	0.05	0.03	0.00	-0.53	-0.44	0.10	-0.06	0.05	-0.08
4.47	0.08	0.00	0.00	0.01	0.02	-0.06	-0.06	-0.08	-0.54	0.49	-0.45	0.50
5.70	0.25	0.08	0.43	0.52	0.40	-0.34	0.29	-0.33	0.05	-0.02	0.04	-0.02
6.03	0.22	-0.51	-0.33	-0.51	0.32	-0.34	0.24	-0.22	0.03	-0.01	0.02	-0.01

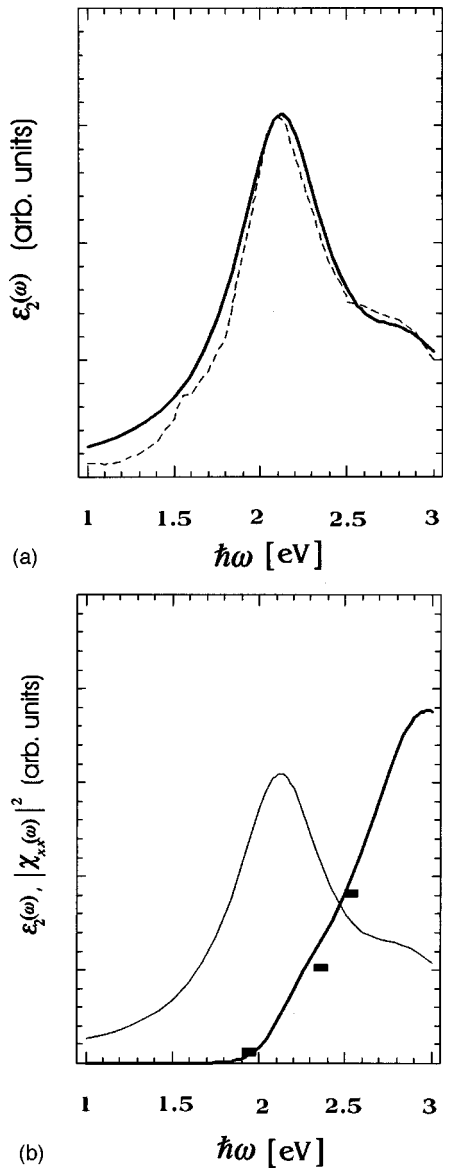

FIG. 3. (a) Experimental and theoretical absorption spectra $\varepsilon_2(\omega)$ of La_2CuO_4. Solid line: theoretical $\varepsilon_2(\omega)$; dotted line (Ref. 1): experimental $\varepsilon_2(\omega)$. (b) Two-magnon Raman intensity $|\chi_{xx}(\omega)|^2$ of La_2CuO_4. Solid line: theoretical $|\chi_{xx}(\omega)|^2$; solid rectangles (Ref. 14): experimental $|\chi_{xx}(\omega)|^2$ in comparison to the theoretical $\varepsilon_2(\omega)$ (thin solid line). $\Gamma_{1,2}=0.32$ eV and $\Gamma_{i>2}=0.34$ eV.

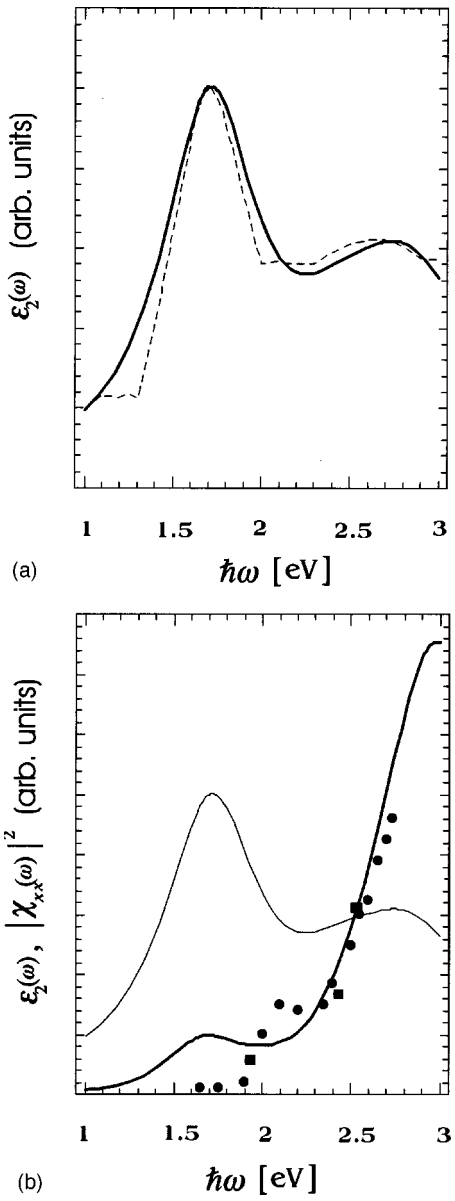

FIG. 4. (a) Experimental and theoretical absorption spectra $\varepsilon_2(\omega)$ of $YBa_2Cu_4O_6$. Solid line: theoretical $\varepsilon_2(\omega)$; dotted line (Ref. 5): experimental $\varepsilon_2(\omega)$. (b) Two-magnon Raman intensity $|\chi_{xx}(\omega)|^2$ of $YBa_2Cu_4O_6$. Solid line: theoretical $|\chi_{xx}(\omega)|^2$; solid rectangles (Ref. 14) and circles (Ref. 15): experimental $|\chi_{xx}(\omega)|^2$ in comparison to the theoretical $\varepsilon_2(\omega)$ (thin solid line). $\Gamma_{1,2}=0.32$ eV and $\Gamma_{i>2}=0.36$ eV.

increases because the optical responses are determined only by the nearest-neighbor states $\Psi^1_{ex+}, \Psi^1_{ex+}(0)$, and $\Psi^1_{ex+}(2)$. In fact, the linear absorption is determined only by the coefficient $a_i[ex]$ of Ψ^1_{ex+}, whereas the enhancement spectrum of two-magnon RS is governed by $b_i[ex]$ and $c_i[ex]$ of $\Psi^1_{ex+}(0)$ and $\Psi^1_{ex+}(2)$ as well as $a_i[ex]$ as seen below in Eqs. (3.1)–(3.8). Spatially separated electron-hole states contribute to the optical responses as the higher-order perturbations in t_0 and t_p. The absorption spectrum of $YBa_2Cu_3O_6$ is almost determined by the eight lowest basis states. Even the enhancement spectrum of the two-magnon RS is determined by the 12 basis states given at the beginning of Sec. II C. Inclusion of further states with larger electron-hole separation corresponding to higher-order perturbation was unnecessary.

B. Absorption spectra

The transition dipole moment to $\Psi_{ex+}[i]$ from the ground state $|g>$, the Néel state, is evaluated as

$$P^x_{gi} \equiv \langle g|P^x|\Psi_{ex+}[i]\rangle = a_i[ex]\mu_x, \tag{3.1}$$

where μ_x is the x component of $\boldsymbol{\mu}_{il}$. Then the imaginary part of the dielectric function $\epsilon_2(\omega)$, which is proportional to the linear absorption spectrum $\alpha(\omega)$, is derived as

$$\varepsilon_2^{xx}(\omega) = 4\pi N_u \mu_x^2 \sum_{i=1} \frac{(a_i[ex])^2\Gamma_i}{(E_i-\omega)^2+\Gamma_i^2}, \tag{3.2}$$

where Γ_i is the transverse relaxation rate of the ith level and N_u is the number density of the unit cells. The calculated absorption spectra together with the experimental spectra are shown for La_2CuO_4 and $YBa_2Cu_3O_6$ in Figs. 3(a) and 4(a), respectively.

As emphasized in Sec. III A, the relative magnitude of the oscillator strength of the lowest-energy bound exciton to the strength on the high-energy side is very sensitive to the relative magnitude of the exciton binding energy V to the effective charge-transfer matrix element t_p. In the case of La_2CuO_4, $V>t_p$, the exciton (bound) state Ψ^1_{ex+} at $E_2=2.12$ eV and the two-magnon excited state $\Psi^1_{ex+}(0)$ at $E_1=1.96$ eV are rather good concepts as shown by the amplitude of $\Psi^1_{ex+}(a_2=0.77)$ and that of $\Psi^1_{ex+}(0)(b_1=0.62)$, respectively. These two states constitute the strong absorption peak on the low-energy side. The unbound states Ψ^2_{ex+} and Ψ^3_{ex+} and their exchanged states $\Psi^2_{ex+}(0)$ and $\Psi^3_{ex+}(0)$ are only weakly hybridized with Ψ^1_{ex+} and $\Psi^1_{ex+}(0)$ and contribute to the weak shoulder on the high-energy side as the second group of states $E_3=2.80$ eV and $E_4=2.85$ eV in the absorption spectrum. Remember that, when the hole $O^-(2p)^5$ with up-spin electron $2p_\sigma\uparrow$ and the electron $Cu^+(3d)^{10}$ on the A sublattice form the bound states, the up-spin electron $2p_\sigma\uparrow$ on $O^-(2p)^5$ can be exchanged with the down-spin electron $3d_{x^2-y^2}\downarrow$ of $Cu^{2+}(3d)^9$ on the B sublattice, and the result is what we call *the exchanged state*.

On the other hand, in $YBa_2Cu_3O_6$, the lowest two states at $E_2=1.73$ eV and $E_1=1.62$ eV are well hybridized with the unbound states Ψ^2_{ex+}, Ψ^3_{ex+}, $\Psi^2_{ex+}(0)$, and $\Psi^3_{ex+}(0)$ and vice versa, as $V=0.35$ eV, here is smaller than $t_p=0.55$ eV. These two levels have an absorption peak on the low-energy side at around 1.7 eV. Three levels at $E_5=2.76$ eV, $E_6=2.85$ eV, and $E_7=2.92$ eV, which consist mainly of Ψ^4_{ex+}, Ψ^3_{ex+}, and Ψ^2_{ex+}, have reasonable magnitudes for transition dipole moments $a_5=0.33$, $a_6=0.19$, and $a_7=0.23$. As a result, the second absorption peak can have a relatively larger oscillator strength than that found in the case of La_2CuO_4. The convergence of the linear absorption spectrum was satisfactory as the inclusion of the unbound state $\Psi^n_{ex+}(n>4)$ gave almost the same spectrum as that obtained by using $\Psi^n_{ex+}(n\leqslant 4)$.

C. Two-magnon RS resonance enhancement

The resonant-enhancement spectrum of two-magnon RS is described by the absolute square of the Raman tensor

$$\chi^{fg}_{xy}(\omega)=\sum_{i\neq g,f}\left\{\frac{P^x_{fi}P^y_{ig}}{E_{ig}-\omega-i\Gamma_i}+\frac{P^y_{fi}P^x_{ig}}{E_{if}+\omega+i\Gamma_i}\right\}, \quad (3.3)$$

where ω denotes the angular frequency of the incident radiation field and E_{if} is lower by two-magnon energy than $E_{ig}=E_i$, the eigenenergy of dipole-allowed excited states $\Psi_{ex+}[i]$. Let us choose $|f\rangle=|f_{\text{2-spin dev.}}\rangle$, and $|g\rangle=|$ Néel $\rangle$ where $|f_{\text{2-spin dev.}}\rangle$ denotes the electronic ground state with two nearest-neighbor spins reversed as compared with the ground state $|$ Néel $\rangle$. Noting Eq. (2.32) and

$$\langle f_{\text{2-spin dev.}}|P^x|\Psi^1_{ex+}(0)\rangle=\mu_x, \quad (3.4)$$

$$\langle f_{\text{2-spin dev.}}|P^x|\Psi^1_{ex+}(2)\rangle=-\mu_x, \quad (3.5)$$

$$\langle f_{\text{2-spin dev.}}|P^x|\Psi^1_{ex+}(1)\rangle=0, \quad (3.6)$$

$$\langle f_{\text{2-spin dev.}}|P^x|\Psi^n_{ex+}\rangle=0 \quad (n\geqslant 2), \quad (3.7)$$

$$\langle f_{\text{2-spin dev.}}|P^x|\Psi^n_{ex+}(0)\rangle=0 \quad (n\geqslant 2), \quad (3.8)$$

we find that the Raman tensor $\chi_{xx}(\omega)$ per unit cell is expressed in terms of $a_i[ex]$, $b_i[ex]$, and $c_i[ex]$ as

$$\chi_{xx}(\omega)=2|\mu_x|^2\sum_{i=1}\frac{a_i[ex](b_i[ex]-c_i[ex])}{E_i-\omega-i\Gamma_i}. \quad (3.9)$$

The Raman tensors in Eqs. (3.3) and (3.9) represent the contribution from a single unit cell in which two inverted spins in the site representation are located in the nearest-neighbor Cu ions, e.g., the mth and nth ion each in the A and B sublattices. We now proceed to the evaluation of the crystal Raman tensor $\chi^{fg}_{\alpha\beta}(\omega)$.[49] For this purpose, we remember that two-magnon RS has usually been described by the following RS Hamiltonian:[10]

$$H_{RS}=-\sum_{\langle mn\rangle}A(\boldsymbol{E}\cdot\boldsymbol{\sigma}_{mn})(\boldsymbol{E}'\cdot\boldsymbol{\sigma}_{mn})\boldsymbol{S}_m\cdot\boldsymbol{S}_n. \quad (3.10)$$

Here the sum $\langle mn\rangle$ is carried out over all the nearest-neighbor pairs, $\boldsymbol{E}$ and $\boldsymbol{E}'$ denote the incident and scattered electric field vectors, respectively, and the vector $\boldsymbol{\sigma}_{mn}$ is the unit vector drawn from site m to its nearest neighbor n. The Hamiltonian H_{RS} is an effective Hamiltonian which is valid within the spin space. Our Raman tensor Eq. (3.3) is then related to the matrix element of this Hamiltonian as follows:

$$\begin{aligned}\langle f|H_{RS}|g\rangle&=-\sum_\alpha P^\alpha_{fg}E'_\alpha\\&=-\sum_{\alpha\beta}E'_\alpha\chi^{fg}_{\alpha\beta}(\omega)E_\beta\\&=-\sum_{\alpha\beta}E'_\alpha E_\beta\sum_{\langle mn\rangle}A(\omega)\\&\quad\times(\boldsymbol{\sigma}_{mn})_\alpha(\boldsymbol{\sigma}_{mn})_\beta\langle f|\boldsymbol{S}_m\cdot\boldsymbol{S}_n|g\rangle, \quad (3.11)\end{aligned}$$

where $|f\rangle$ and $|g\rangle$ are any pair of states within the manifold of Cu^{2+} spins. The expression P^α_{fg} on the right-hand side of the first line represents the transition moment associated with the excitation from $|g\rangle$ to $|f\rangle$, which is induced by the incident electric field. On the second line, this expression is replaced by $\Sigma_\beta\chi^{fg}_{\alpha\beta}(\omega)E_\beta$ in accordance with the definition of the susceptibility tensor. We thus find the following relation:

$$\chi^{fg}_{\alpha\beta}(\omega)=\sum_{\langle mn\rangle}A(\omega)(\boldsymbol{\sigma}_{mn})_\alpha(\boldsymbol{\sigma}_{mn})_\beta\langle f|\boldsymbol{S}_m\cdot\boldsymbol{S}_n|g\rangle. \quad (3.12)$$

When we treat the two-magnon RS, we expand the spin operators $\boldsymbol{S}^-_m$ (A sublattice) and $\boldsymbol{S}^+_n$ (B sublattice) in terms of the magnon operators $\alpha_{\boldsymbol{k}}$ and $\beta_{\boldsymbol{k}}$ through the Fourier transform and Bogoliubov transformation as

$$S_{A\boldsymbol{k}}^{-}=\frac{1}{\sqrt{N_u}}\sum_{m\in A} S_m^{-}\exp(i\boldsymbol{k}\cdot\boldsymbol{R}_m)=\sqrt{2S}(u_{\boldsymbol{k}}\alpha_{\boldsymbol{k}}^{\dagger}+v_{\boldsymbol{k}}\beta_{\boldsymbol{k}}), \tag{3.13}$$

$$S_{B-\boldsymbol{k}}^{+}=\frac{1}{\sqrt{N_u}}\sum_{n\in B} S_n^{+}\exp(-i\boldsymbol{k}\cdot\boldsymbol{R}_n)=\sqrt{2S}(u_{\boldsymbol{k}}\beta_{-\boldsymbol{k}}^{\dagger}+v_{\boldsymbol{k}}\alpha_{-\boldsymbol{k}}), \tag{3.14}$$

with $S=1/2$ in the present problem. Here the coefficients $u_{\boldsymbol{k}}$ and $v_{\boldsymbol{k}}$ in the Bogoliubov transformation obey $|u_{\boldsymbol{k}}|^2-|v_{\boldsymbol{k}}|^2=1$, and the summation $m(n)$ runs over the A (B) sublattice. Then the RS Hamiltonian equation (3.10) is rewritten in terms of the magnon operators as follows:

$$H_{RS}=-\sum_{\boldsymbol{k}} A(\omega)SF_{\alpha\beta}(\boldsymbol{k})(u_{\boldsymbol{k}}^2+v_{\boldsymbol{k}}^2)\alpha_{\boldsymbol{k}}^{\dagger}\beta_{-\boldsymbol{k}}^{\dagger}, \tag{3.15}$$

where we have kept only those terms that lead to the two-magnon excitation from the ground zero-magnon state $|0\rangle$. The trigonometric factor $F_{\alpha\beta}(\boldsymbol{k})$ is defined by

$$F_{\alpha\beta}(\boldsymbol{k})=\sum_{n} (\boldsymbol{\sigma}_{mn})_{\alpha}(\boldsymbol{\sigma}_{mn})_{\beta}\exp(ia\boldsymbol{k}\cdot\boldsymbol{\sigma}_{mn}), \tag{3.16}$$

where a is the distance between the nearest pair of Cu^{2+} ions. When we choose the zero-magnon state $|0\rangle$ as the ground state $|g\rangle$ and two-magnon state $|\boldsymbol{k},-\boldsymbol{k}\rangle=\alpha_{\boldsymbol{k}}^{\dagger}\beta_{-\boldsymbol{k}}^{\dagger}|0\rangle$ as the final state $|f\rangle$, we have the crystalline Raman tensor $\chi_{\alpha\beta}^{fg}(\omega)$ expressed as

$$\begin{aligned}\chi_{\alpha\beta}^{fg}(\omega_i)&\equiv\chi_{\alpha\beta}(\omega_s,\boldsymbol{k},-\boldsymbol{k};\omega_i,0)\\&=A(\omega_i)SF_{\alpha\beta}(\boldsymbol{k})(u_{\boldsymbol{k}}^2+v_{\boldsymbol{k}}^2).\end{aligned} \tag{3.17}$$

Here let us remember that the final state $|f\rangle$ contains two magnons with their wave vector and energy, $(\boldsymbol{k},\omega_{\boldsymbol{k}})$ and $(-\boldsymbol{k},\omega_{-\boldsymbol{k}})$. We may neglect here the wave vectors of the incident light $\omega_i\equiv\omega$ and scattered one ω_s in comparison with that of the magnon, i.e., $\boldsymbol{k}$. See Ref. 49 for the trigonometric factor $F_{\alpha\beta}(\boldsymbol{k})$. Then the spectrum $I_{\alpha\beta}(\omega_s,\omega_i)$ of two-magnon Raman scattering can be described in terms of the Raman tensor of Eq. (3.17) excluding an unimportant factor as

$$\begin{aligned}&I_{\alpha\beta}(\omega_s,\omega_i)\\&=\sum_{\boldsymbol{k}}|\chi_{\alpha\beta}(\omega_s,\boldsymbol{k},-\boldsymbol{k};\omega_i,0)|^2\delta(\omega_s+E_f-\omega_i-E_g)\\&=|A(\omega_i)|^2\sum_{\boldsymbol{k}} S^2F_{\alpha\beta}^2(\boldsymbol{k})(u_{\boldsymbol{k}}^2+v_{\boldsymbol{k}}^2)^2\\&\quad\times\delta(\omega_s+\omega_{\boldsymbol{k}}+\omega_{-\boldsymbol{k}}-\omega_i).\end{aligned} \tag{3.18}$$

After integrating $I_{\alpha\beta}(\omega_s,\omega_i)$ over the scattering frequency ω_s, the resonance-enhancement spectrum is found to be given by $|A(\omega_i)|^2$. Furthermore, we can correlate the factor $A(\omega)$ to $\chi_{xx}(\omega)$ of Eq. (3.9) by setting $|f\rangle=|f_{\text{2-spin dev.}}\rangle$ and $|g\rangle=|$ Néel $\rangle$ on both sides of Eq. (3.12) so that

$$\chi_{xx}(\omega)=A(\omega)S. \tag{3.19}$$

The most interesting problem of this strong two-magnon RS is the mystery of why this RS is not resonantly enhanced even when the incident light frequency ω approaches the first exciton peak but it is strongly enhanced for ω close to the higher-energy levels. We are not interested here in the two-magnon RS spectrum itself but in the problem of how the total intensity of two-magnon RS is enhanced when the incident light ω is resonant to the higher excited levels. To solve this problem, information on magnon dispersion is not necessary and it will be sufficient to point out that this enhancement spectrum can be described by the absolute square of the Raman tensor given by Eq. (3.9) as shown by Eq. (3.17). This point was justified in Ref. 49 as long as the exchange interaction in the second order of t_0, i.e., t_1, t_1', t_2, and t_2', is much larger than $J/4$, i.e., the fourth-order expansion in t_0. This is the case of our cuprates as the value $J/4$ is by an order of magnitude smaller than t_1, t_1', t_2, and t_2'.

Raman scattering due to single or double phonons has been described traditionally by expanding the basic Raman tensor of Eq. (3.3) to the first or second orders in the intraband electron-phonon interactions. Chubukov and Frenkel[43] expanded the basic Raman tensor in a similar manner in terms of the intraband fermion-magnon interaction to the second order assuming the band-to-band electronic transition of the single-band Mott-Hubbard model to be involved in the resonance enhancement. However, in the present cuprates, relevant electronic excitations in the visible region are known to originate in the charge-transfer from $O(2p_{\sigma})$ to the empty $Cu(3d_{x^2-y^2})$ orbital, and two-magnon excited states are strongly hybridized with the dipole-allowed excited states. Therefore, it seems reasonable for us to take into account these two-magnon excited states $\{\Psi_{ex+}^1(0),\Psi_{ex+}^1(2),\Psi_{ex+}^1(1),\Psi_{ex+}^2(0),\ldots\}$ from the very beginning in describing the electronic excited states of these systems as has been done in the present paper. As a result, we can describe two-magnon RS by the basic Raman tensor itself without resorting to the perturbational expansion of the intraband fermion-magnon interaction. From the present point of view, this is also the reason why strong two-magnon RS has been observed in these cuprates.

The resonance-enhancement spectra of two-magnon RS are given for La_2CuO_4 and $YBa_2Cu_3O_6$ in Figs. 3(b) and 4(b), respectively. The resonance-enhancement spectrum of two-magnon RS in La_2CuO_4 may be understood as follows: the lowest two levels, which are made of mainly $\Psi_{ex+}^1(0)$ and Ψ_{ex+}^1, are well mixed up with each other by $-t_2'=t_0^2/(E_p+U_p+V)$, and the lowest level is also hybridized with the unbound state Ψ_{ex+}^2 through t_p, i.e., $e_1=-0.46$. As a result, the Raman tensor due to the mainly dipole-allowed state E_2, $a_2\times(b_2-c_2)=0.77\times0.21$, has the opposite sign from those of the lowest E_1 and from the third level E_3, $a_1\times(b_1-c_1)=-0.12\times0.41$ and $a_3\times(b_3-c_3)=-0.20\times0.48$, respectively. Therefore, the contribution of the dipole-allowed state E_2 to the Raman tensor is almost canceled out by those of E_1 and E_3 around and below the low-energy absorption peak as shown in Fig. 3(b). The high-energy states at $E_3=2.80$ eV, $E_4=2.86$ eV, and $E_5=3.02$ eV, which constitute the shoulder on the high-energy side of the absorption spectrum, have a reasonable magnitude of dipole-allowed components $a_3=0.20$, $a_4=0.30$, and

$a_6=0.19$. Additionally, the states have large two-magnon components $(b_3-c_3)=-0.48$, $(b_4-c_4)=-0.32$, $(b_5-c_5)=-0.84$ because of the charge-transfer effects t_p and t_0^2. These three components contribute additively to the two-magnon RS so that the resonance enhancement is clearly observed only when the incident frequency is close to the high-energy shoulder in La_2CuO_4.

On the other hand, in $YBa_2Cu_3O_6$ the lowest two states at $E_2=1.73$ eV and $E_1=1.62$ eV are well hybridized with the unbound states Ψ^2_{ex+}, Ψ^3_{ex+}, $\Psi^2_{ex+}(0)$, and $\Psi^3_{ex+}(0)$ as $V=0.35$ eV is smaller than $t_p=0.55$ eV. The contribution to two-magnon RS from the mainly dipole-allowed state $E_2, a_2\times(b_2-c_2)=-0.60\times 0.08$, not only has a reduced two-magnon component, but it is almost canceled out by the lowest E_1 and the third lowest E_3 states, i.e., $a_1\times(b_1-c_1)=0.30\times 0.44$ and $a_3\times(b_3-c_3)=0.24\times 0.26$, around and below the absorption peak on the low-energy side around 1.7 eV. The three states at $E_4=2.76$ eV, $E_5=2.85$ eV, and $E_5=2.92$ eV, whose main components are Ψ^4_{ex+}, Ψ^3_{ex+}, Ψ^2_{ex+}, and $\Psi^1_{ex+}(2)$, can have enough large magnitude of dipole moments $a_4=0.25$, $a_5=0.33$, and $a_6=0.19$ as well as the two-magnon components $b_4-c_4=-0.20$, $b_5-c_5=-0.22$, and $b_6-c_6=-0.41$. As a result, the second absorption peak has a larger oscillator strength than for La_2CuO_4 and a much stronger resonance enhancement of two-magnon RS on the high-energy side is observed because these three levels contribute additively to the two-magnon RS in both crystals.

IV. DISCUSSION

We have examined the contribution of bound and unbound excitations to the linear light absorption and the resonance-enhancement spectra of two-magnon RS in La_2CuO_4 and $YBa_2Cu_3O_6$ using the site representation as bases. These spectra were found to be sensitive to the relative magnitude of the exciton binding force V and the hole-transfer integral t_p which determines the relative importance of the bound and unbound states of the electron $Cu^+(3d)^{10}$ and the hole $O^-(2p)^5$ on the CuO_2 plane. First, we have understood the different distributions of the oscillator strength between the low- and high-energy sides in the visible region of La_2CuO_4 and $YBa_2Cu_3O_6$. Second, we have found that the exchange processes between $O^-2p_\sigma\uparrow(\downarrow)$ and its nearest-neighbor $Cu^{2+}3d_{x^2-y^2}\downarrow(\uparrow)$ electrons in the optically excited state induces the two-magnon excited state strongly in the second-order processes in t_0. This is the reason for the strong two-magnon RS. Third, we have shown that the resonance enhancement of two-magnon RS can be almost vanishing around and below the lowest-energy absorption peak while it is enhanced on the high-energy second absorption peak or shoulder because the two levels which give rise to the first peak may have contributions of the opposite sign to the two-magnon RS, while the three levels composing the second absorption peak contribute additively to two-magnon RS.

In the present paper, we confined ourselves to the calculation of the E_u symmetry states which are involved in the absorption and two-magnon RS. When we repeat this calculation for the states with A_{1g}, B_{1g}, A_{2g}, and B_{2g} symmetry of D_{4h}, we will be able to understand the large-shift RS. This is a future problem.

We have evaluated only the elementary excitations with wave vector $\boldsymbol{k}\doteq 0$ which the visible light can excite, taking into account the AF A and B sublattices. Reciprocal-lattice points on the Brillouin-zone boundary in the usual band calculation which neglects the AF structure are folded onto the Γ point of the AF Brillouin zone. Therefore, we may expect that the energy separation between the highest and lowest energies in the present calculation gives the dispersion width of our elementary excitations. As seen in Tables III and IV, La_2CuO_4 and $YBa_2Cu_3O_6$ have energy widths of 3.9 and 4.4 eV, respectively. These values are very close to the hole band widths of $8t_p=4.0$ eV and 4.4 eV,[30,31,36,38] respectively. On the other hand, the exciton band width is estimated as $2t_p[t_0/(E_p+U_p)]^2=10$ meV and 40 meV for La_2CuO_4 and $YBa_2Cu_3O_6$, respectively. Deriving the dispersion relation of the bound as well as unbound electron-hole pair in the present model is also a future problem.

Now that eigenfunctions and eigenenergies of the low-lying electronic excitations have been obtained for these systems, it should also be possible to evaluate some of the nonlinear optical responses in these systems. This too is another future problem.

ACKNOWLEDGMENTS

One of the authors (E.H.) thanks Professor M. V. Klein, Professor Y. Tokura, and Professor S. Uchida for fruitful discussions and important information relevant to the present calculation.

[1] Y. Tokura, S. Koshihara, T. Arima, H. Takagi, S. Ishibashi, T. Ido, and S. Uchida, Phys. Rev. B **41**, R11 657 (1990).
[2] T. Arima, K. Kikuchi, M. Kasuya, S. Koshihara, Y. Tokura, T. Ido, and S. Uchida, Phys. Rev. B **44**, R917 (1991).
[3] Tineke Tio, R.J. Birgeneau, A. Cassanko, and M.A. Kasten, Phys. Rev. B **42**, R10 800 (1990).
[4] J.P. Falck, A. Levy, M.A. Kastner, and R.J. Birgeneau, Phys. Rev. Lett. **69**, 1109 (1992).
[5] H. Romberg, N. Nücker, J. Fink, Th. Wolf, X.X. Xi, B. Koch, H.P. Geserich, M. Dürrler, W. Assmus, and B. Gegenheimer, Z. Phys. B: Condens. Matter **78**, 367 (1990).
[6] S.L. Cooper, G.A. Thomas, A.J. Millis, P.E. Sulewski, J. Orenstein, D.H. Rapkine, S-W. Cheong, and P.L. Trevor, Phys. Rev. B **42**, R10 785 (1990).
[7] S.L. Cooper, D. Reznik, A. Kotz, M.A. Karlov, R. Liu, M.V. Klein, B.W. Veal, and A.P. Paulikas, Phys. Rev. B **47**, 8233 (1993).
[8] S. Sugai, Phys. Rev. B **39**, 4306 (1989).
[9] E.T. Heyen, J. Kircher, and M. Cardona, Phys. Rev. B **45**, 3037 (1992).
[10] K.B. Lyons, P.A. Fleury, L.F. Schneemeyer, and J.V. Waszczak, Phys. Rev. Lett. **60**, 732 (1988).
[11] K.B. Lyons, P.A. Fleury, J.P. Remeika, A.S. Cooper, and T.J. Negran, Phys. Rev. B **37**, 2353 (1988).

[12] K.B. Lyons, P.E. Sulewski, P.A. Fleury, H.L. Carter, A.S. Cooper, G.P. Espinosa, Z. Fish, and S-W. Cheong, Phys. Rev. B **39**, R9693 (1989).
[13] S. Sugai, S. Shamoto, and M. Sato, Phys. Rev. B **38**, 6436 (1988).
[14] M. Yoshida, S. Tajima, N. Koshizuka, S. Tanaka, S. Uchida, and T. Itoh, Phys. Rev. B **46**, 6505 (1992).
[15] R. Liu, M.V. Klein, D. Salamon, S.L. Cooper, W.C. Lee, S-W. Cheng, and D.M. Ginsberg, J. Phys. Chem. Solids **54**, 1347 (1993).
[16] P. Knoll, M. Mayer, W. Brenig, and Ch. Waidacher, J. Low Temp. Phys. **105**, 383 (1996).
[17] G. Blumberg, P. Abbamonte, M.V. Klein, W.C. Lee, D.M. Ginsberg, L.L. Miller, and A. Zibold, Phys. Rev. B **53**, R11 930 (1996).
[18] R. Liu, D. Salamon, M.V. Klein, S.L. Cooper, W.C. Lee, S-W. Cheng, and D.M. Ginsberg, Phys. Rev. Lett. **71**, 3709 (1993).
[19] D. Salamon, R. Liu, M.V. Klein, M.V. Karlow, S.L. Cooper, S-W. Cheng, W.C. Lee, and D.M. Ginsberg, Phys. Rev. B **51**, 6617 (1995).
[20] V.N. Denisov, C. Taliani, A.G. Mal'shukov, V.M. Burlakov, E. Schönherr, and G. Ruani, Phys. Rev. B **48**, 16 714 (1989).
[21] I. Ohana, D. Heiman, M.S. Dresselhaus, and P.J. Picone, Phys. Rev. B **40**, 2225 (1989).
[22] G. Yu, C.H. Lee, D. Mihailovich, A.J. Heeger, C.F. Fincher, N. Herron, and E.M. McCarron, Phys. Rev. B **48**, 7545 (1993).
[23] N. Nücker, H. Romberg, X.X. Xi, J. Fink, B. Gegenheimer, and Z.X. Zhao, Phys. Rev. B **39**, 6619 (1989).
[24] C.T. Chen, F. Sette, Y. Ma, M.S. Hybertsen, E.B. Stechel, W.M.C. Foulkes, M. Schluter, S-W. Cheong, A.S. Cooper, L.W. Rupp, Jr., B. Batlogg, Y.L. Soo, Z.H. Ming, A. Knol, and Y.H. Kao, Phys. Rev. Lett. **66**, 104 (1991).
[25] B.O. Wells, Z.-X. Shen, A. Matsuura, D.M. King, M.A. Kastner, M. Greven, and R.J. Birgeneau, Phys. Rev. Lett. **74**, 964 (1995).
[26] Y.Y. Wang, F.C. Zhang, V.P. Dravid, K.K. Ng, M.V. Klein, S.E. Schnatterly, and L.L. Miller, Phys. Rev. Lett. **77**, 1809 (1996).
[27] J.J.M. Pothuizen, R. Eder, N.T. Hien, M. Matoba, A.A. Menovsky, and G.A. Sawatzky, Phys. Rev. Lett. **78**, 717 (1997).
[28] L.C. Duda, G. Dräger, S. Tanaka, A. Kotani, J. Guo, D. Heumann, S. Bocharov, N. Wassdahl, and J. Nordgren, J. Phys. Soc. Jpn. **67**, 416 (1998).
[29] P. Kuiper, J.H. Guo, C. Sathe, L.C. Duda, and J. Nordgren, Phys. Rev. Lett. **80**, 5204 (1998).
[30] F. Herman, R.V. Kasowski, and V.Y. Hsu, Phys. Rev. B **36**, 6904 (1987).
[31] A.K. McMahan, R.M. Martin, and S. Satpathy, Phys. Rev. B **38**, 6650 (1988).
[32] F.C. Zhang and T.M. Rice, Phys. Rev. B **37**, R3759 (1988).
[33] M. Ogata and H. Shiba, J. Phys. Soc. Jpn. **57**, 3074 (1988).
[34] H. Matsukawa and H. Fukuyama, J. Phys. Soc. Jpn. **59**, 1723 (1990); **58**, 3687 (1989); **58**, 2845 (1989).
[35] H. Fukuyama, H. Matsukawa, and Y. Hasegawa, J. Phys. Soc. Jpn. **58**, 364 (1989).
[36] L.F. Mattheiss and D.R. Hamann, Phys. Rev. B **40**, 2217 (1989).
[37] R.R.P. Singh, P.A. Fleury, K.B. Lyons, and P.E. Sulewski, Phys. Rev. Lett. **62**, 2736 (1989).
[38] H. Eskes, L.H. Tjeng, and G.A. Sawatzky, Phys. Rev. B **41**, 288 (1990).
[39] P.E. Sulewski, P.A. Fleury, K.B. Lyons, S-W. Cheong, and Z. Fish, Phys. Rev. B **41**, 225 (1990).
[40] B.S. Shastry and B.I. Shraiman, Phys. Rev. Lett. **65**, 1068 (1990); Int. J. Mod. Phys. B **5**, 365 (1991).
[41] J.B. Grant and A.K. McMahan, Phys. Rev. Lett. **66**, 488 (1991).
[42] H. Eskes and G.A. Sawatzky, Phys. Rev. B **44**, 9656 (1991).
[43] A.V. Chubukov and D.M. Frenkel, Phys. Rev. Lett. **74**, 3057 (1995).
[44] D.K. Morr, A.V. Chubukov, A.P. Kamph, and G. Blumberg, Phys. Rev. B **54**, 3468 (1996).
[45] F.C. Zhang and K.K. Ng, Phys. Rev. B **58**, 13 520 (1998).
[46] M.E. Simon, A.A. Aligia, C.D. Batista, E.R. Gagliano, and F. Lema, Phys. Rev. B **54**, R3780 (1996).
[47] M. Muto, Y. Tanabe, T. Iizuka-Sakano, and E. Hanamura, Phys. Rev. B **57**, 9586 (1998).
[48] Y. Tanabe, M. Muto, F. Fiebig, and E. Hanamura, Phys. Rev. B **58**, 8654 (1998).
[49] E. Hanamura, Y. Tanabe, and N.T. Dan, J. Lumin. **83/84**, 19 (1999).
[50] E. Dagoto, Rev. Mod. Phys. **66**, 763 (1991).
[51] P. Fulde, *Electron Correlations in Molecules and Solids*, 3rd ed., Springer Series in Solid-State Sciences Vol. 100 (Springer-Verlag, Berlin, 1995).
[52] M.S. Hybertsen, E.B. Stechel, W.M.C. Foulkes, and M. Schlüter, Phys. Rev. B **45**, 10 032 (1992).
[53] F. Mila, Phys. Rev. B **38**, 11 358 (1988).